Thermal Management of Surface Mount Power Magnetic Components

G. Refai-Ahmed[1]
Mem. ASME,
Astec Advanced Power Systems Ltd.,
Power Group, MS. 042, 185 Corkstown Rd.,
Nepean, Ontario, K2H 8V4 Canada

M. M. Yovanovich
Fellow ASME,
Department of Mechanical Engineering,
University of Waterloo,
Waterloo, Ontario, N2L 3G1 Canada

A numerical and experimental study of conduction heat transfer from low power magnetic components with gull wing leads was conducted to determine the effects of distributing the power loss between the core, the winding and the thermal underfill on the thermal resistance. The numerical study was conducted in the power loss ratio range of $0.5 \leq PR \leq 1.0$, where the only active power loss was from the winding at $PR=1$. In addition, the effect of the thermal underfill material between the substrate and the lower surface of the magnetic package on the thermal performance of the magnetic device was also examined. For comparison, a test was conducted on a magnetic component at $PR=1$, without thermal underfill. This comparison revealed good agreement between the numerical and experimental results. Finally, a general model was proposed for conduction heat transfer from the surface mount power magnetic packages. The agreement between the model and the experimental results was within 8 percent. [S1043-7398(00)00704-0]

Introduction

In the present microelectronics industrial revolution, designers need to develop technology for high density surface mounting. This can allow them to design circuits with more flexibility and accuracy. One way to power the circuits is by using a primary power supply to power the overall system, which will in turn power the microprocessor devices cards through several low scale power supplies. This low scale power supply is commonly named as a point of used power supply, PUPS. The PUPS can be placed very close to the microprocessor devices. As a result it has received more attention from the microprocessor developers. The main function of these PUPS is to provide the microprocessor with a significant amount of electrical current at a very low output voltage. It is expected that the next generation of high-speed microprocessors will require an input voltage of 0.5 V. This lower scale of the output voltage from the PUPS will produce a significant impact on the heat losses from the PUPS. Therefore, it is very important to improve the thermal performance of the PUPS in order to increase its efficiency and reduce the thermal wake effect from the PUPS to the neighborhood devices. One of the key factors of improving the thermal and the electrical performance is the magnetic components.

One of the commonly used components in the PUPS designs is the surface mount power magnetic component with gull wing leads, which is described in Fig. 1 (the industrial name for this series is ER surface mount). More details on this series can be found in TDK [1]. Therefore, the magnetic designers have an interest in predicting the operating surface temperature of this series. Through this, the engineers can choose the appropriate thermal class of this magnetic series, where the thermal classes A, B, F, and H have maximum surface temperature specifications of 378 K, 403 K, 423 K, and 453 K respectively, in the first stage of the design. These thermal classes refer to different types of electrical insulations for the winding wires. Unfortunately, there is a lack of information concerning the thermal management of magnetic components in the literature. Therefore, the main objective of this study is to investigate the thermal performance of the surface mount power magnetic component with gull wing leads. This study will then lead to a conduction heat transfer model for ER surface mount series. This model can provide a quick way to predict the surface temperature of the ER surface mount series. Furthermore, this investigation examines the effect of the thermal underfill material on the thermal performance of the magnetic device. This concept of using thermal underfill material to eliminate the air gap between a device and the printed board has been used in the electronic packaging. This approach is used to improve the thermal and thermo-mechanical performance of a particular device. However, this type of packaging can add unnecessary costs to the final product, if the thermal performance is

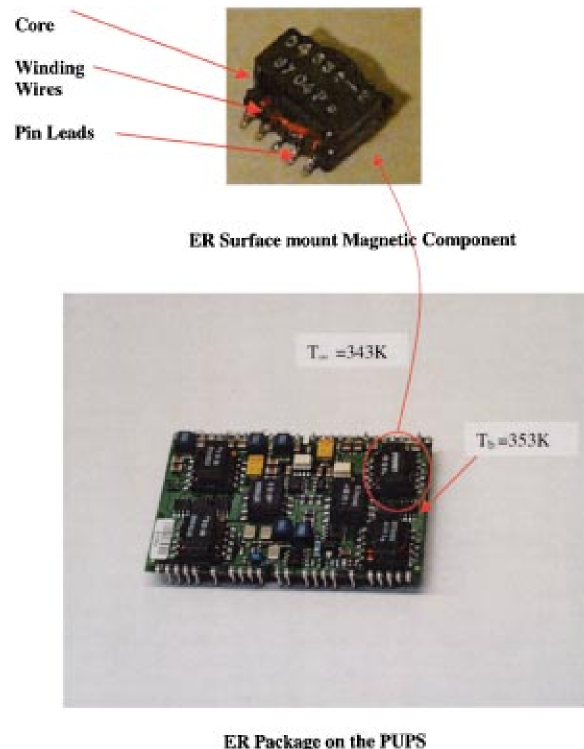

Fig. 1 Photograph of ER package and its location on the PUPS

[1]Present address: Cisco Systems, 365 March Rd., Kamata, Ontario, K2K 2C0 Canada.

Contributed by the Electrical and Electronic Packaging Division for publication in the JOURNAL OF ELECTRONIC PACKAGING. Manuscript received by the EEPD Division November 25, 1999. Associate Technical Editor: Y. Joshi.

 Copyright © 2000 by ASME

improved slightly. Therefore, the present study examines the effect of the thermal underfill material to enhance the thermal performance of the magnetic device.

Numerical Model and Results

The current study examined the conduction heat transfer from ER packages to the substrate. The substrate surface temperature under the ER package was assumed constant, which is the Dirichlet boundary condition. Moreover, the convection and radiation heat transfer from the ER packaging were neglected in this analysis. This assumption is valid when the top side of the power supply is bounded with either a plastic cover or an electromagnetic shield. This means that the shield or the plastic cover can be defined as an adiabatic boundary. Therefore, the effect of the internal convection between the top side of the power supply and the shield or the plastic cover was assumed negligible. The radiation heat transfer is also negligible in the case of the electromagnetic shield and the top surface of the power supply, as well as, the glass reinforced nylon cover and the top surface of the power supply.

Therefore, it was assumed that the heat was transferred by conduction from the ER package to the substrate and the surrounding air. The validity of the present assumptions will be verified by comparing the numerical results with the experimental data.

Figure 2 shows a schematic diagram of the numerical model of the ER package. It also reveals the dimensions of the numerical model and the boundary conditions.

The present investigation solved the elliptic partial differential equation of the steady-state heat conduction equation in three dimensions.

$$\nabla^2 T = 0 \quad (1)$$

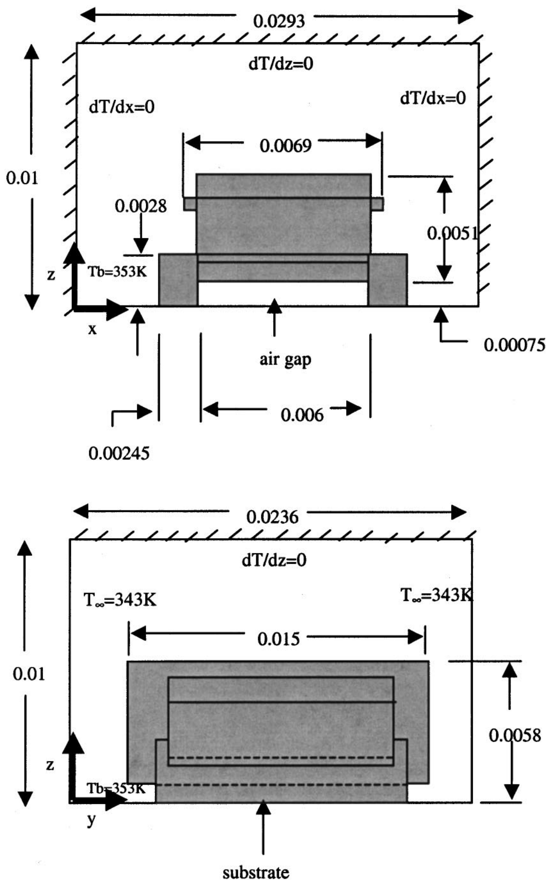

Fig. 2 Schematic diagram of numerical model of ER package (all dimensions in m)

A finite volume based commercial software Flotherm [2] was used. Grid accuracy was verified by doubling the number of the grids within the numerical domain in all directions. A typical grid uses 31, 24, and 27 cells in x, y, and z directions. The numerical domain dimensions in x, y, and z were 0.0293 m, 0.0236 m and 0.01 m, respectively. The predicated temperature changed by about 0.87 percent between the two types of grids. Therefore, the typical grid provides sufficient numerical accuracy.

The numerical solutions were conducted for ER 14.5 package with and without thermal underfill material. The thermal conductivity of the thermal underfill material was defined as 0.8 W/m.K. The ambient air and the substrate temperatures were assumed to be 343 K and 353 K, respectively. The surrounding air temperature, 343 K, is a typical worst environment temperature scenario for these applications. The left, right, and top walls in xz-plane were adiabatic boundaries. These boundaries represent the glass reinforced nylon cover on the power supply. However, the left and the right walls in yz-plane were maintained at the ambient air temperature of the power supply. This should allow a thermal link between the ER package and the surrounding components. In addition, the bottom wall in yz-plane was maintained at a constant temperature representing the substrate. Figure 1 describes the location of the magnetic component on the PUPS. It also shows the substrate temperature, T_b, and the local ambient temperature, T_∞. These values are used as boundary conditions in the present component level analysis. These temperatures can be determined from the thermal analysis of the power supply's board. In addition, Fig. 2 reveals the imposed boundary conditions in the schematic diagram of the numerical model.

The effective surface area of the heat dissipation from the core was defined as the side surface area of the core's bobbin. However, the effective surface area of the heat dissipation from the winding was defined as 80 percent of the maximum side area of the winding's bobbin, where the winding coil is covering 80 percent of the outer winding's bobbin diameter. This represents the typical winding surface area. Table 1 shows the effective surface area of the heat dissipation from the winding and the core of the ER surface mount series based on the manufacturers catalogues. These surface areas have a manufacturer tolerance of ± 10 percent.

In addition, the present investigation examined the effect of distributing the power losses between the winding and the core of the package. Therefore, winding loss to total power loss, PR, was varied between 0.5 to 1.0 where the ER package is working as an inductor if PR=1, and as a transformer if PR<1. Moreover, the typical minimum ratio of PR in this type of application is 0.5. This means that 50 percent of the power is dissipated from the core and the other 50 percent from the winding.

Finally, the results from the conduction heat transfer model are expressed in terms of the nondimensional groups of the power loss, the thermal resistance and the nondimensional temperature. This should assist in developing an empirical correlation with these parameters. The next section will define the nondimensional groups of the power loss, thermal resistance and temperature.

Table 1 Effective surface area of heat dissipation from winding and core of ER surface mount series

Package type	Winding* 10^6 (m^2)	Core* 10^6 (m^2)
ER9.5/5	22.40	27.25
ER11/3.9	39.45	35.78
ER11/5	41.65	40.87
ER14.5/6	63.20	54.60

Definitions of Nondimensional Groups

Thermal conductances through the winding and the core are

$$\frac{P_W}{T_S - T_\infty} \quad \text{winding}$$

$$\frac{P_C}{T_S - T_\infty} \quad \text{core}$$

and the total thermal conductances through the magnetic component is

$$\frac{P}{T_S - T_\infty}$$

In this application, the thermal management strategy is to transfer most of the dissipated power from the ER package to the substrate by conduction. Therefore, T_b should be greater than T_∞, except for a very small dissipated power when $T_b \simeq T_\infty$. In the numerical model both T_∞ and T_b were defined. However, in the real application only T_∞ is defined. Therefore, T_∞, was chosen as a reference temperature. Moreover, the relationship between T_∞ and T_b will be determined empirically in the experimental results section. The nondimensional form of the total thermal conductance can be written as follows

$$P^* = \frac{P}{(T_S - T_\infty)k\sqrt{A}} = \frac{P_W}{(T_S - T_\infty)k\sqrt{A_W}}\sqrt{\frac{A_W}{A}} + \frac{P_C}{(T_{S,C} - T_\infty)k\sqrt{A_C}}\sqrt{\frac{A_C}{A}}$$

The values of P_W and P_C can be obtained from the electromagnetic calculation (more details are given in Dixon [3]). Moreover, the ratio of $(A_W/A)^{0.5}$ and $(A_C/A)^{0.5}$ can be approximated as 0.7, where $(A_W/A)^{0.5}$ and $(A_C/A)^{0.5}$ are varied between 0.68 and 0.74 for ER surface mount series. In addition, both the core and winding surface areas have a manufacturer tolerance of 10 percent, as mentioned earlier. Therefore, the total nondimensional thermal conductance, P^*, can be simplified as follows

$$P^* = \frac{0.7P_W}{(T_S - T_\infty)k\sqrt{A_W}} + \frac{0.7P_C}{(T_S - T_\infty)k\sqrt{A_C}} \tag{2}$$

The nondimensional form of the thermal resistance is

$$R^* = \frac{1}{P^*} = \frac{k(T_S - T_\infty)}{0.7P\left[\frac{\text{PR}}{\sqrt{A_W}} + \frac{1-\text{PR}}{\sqrt{A_C}}\right]} \tag{3}$$

where PR is the power loss ratio of winding power loss, P_W to total power loss of the magnetic package, and the total power loss, P, is the summation of P_W and P_C. Finally, the nondimensional temperature can be defined as

$$\theta = \frac{T_S - T_\infty}{T_S - T_b} \tag{4}$$

Discussion of the Results

Figures 3 and 4 show the relationship between the nondimensional thermal resistance, R^*, and the nondimensional temperature, θ, for the present numerical model with and without thermal underfill material. Figure 3 shows that the nondimensional thermal resistance for different power loss ratios is approaching ∞ when $\theta \to \infty$. This means that $k\,(T_S - T_\infty)\sqrt{A}$ (where $\sqrt{A_C} \simeq \sqrt{A_W} \simeq 0.7\sqrt{A}$) is much greater than the power loss. Therefore, the surface temperature, T_S, is almost equal to the substrate temperature, T_b. The numerical results in Figs. 3 and 4 can be correlated for different PR as follows

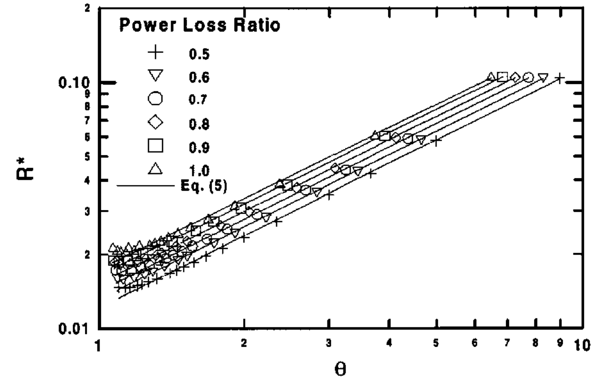

Fig. 3 Relationship between R^* and θ for ER14.5 with thermal underfill

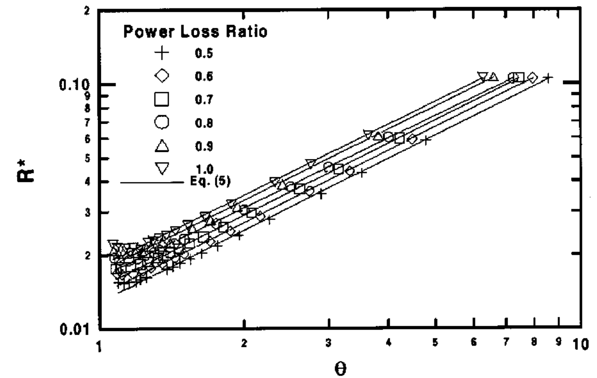

Fig. 4 Relationship between R^* and θ for ER14.5 without thermal underfill

$$R^* = C_1\theta^m \tag{5}$$

Table 2 shows the numerical values of the coefficients C_1 and m for the power loss ratio range between 0.5 to 1.0. Figure 4 also shows the relationship of R^* and θ for the numerical model of the ER package without thermal underfill material. This figure also reveals a similar trend for the relationship between R^* and θ.

One can conclude from Figs. 3 and 4 that the nondimensional thermal resistance is a function of the power loss ratio and the nondimensional temperature, θ. Therefore, the present study developed general models for R^* as a function of PR and θ. Equations (6) and (7) give the nondimensional thermal resistance, R^*, with and without thermal underfill material.

Table 2 Numerical values of constants in Eq. (5) for ER package

PR	$C1\times10^{3+}$	m^+	$C1\times10^{3*}$	m^*
0.5	12.89	0.971	12.09	0.979
0.6	13.83	0.973	13.13	0.977
0.7	14.86	0.973	14.19	0.974
0.8	16.29	0.940	15.29	0.969
0.9	17.14	0.960	16.43	0.966
1.0	18.14	0.958	17.43	0.956

+ER Package with thermal underfill
*ER Package without thermal underfill

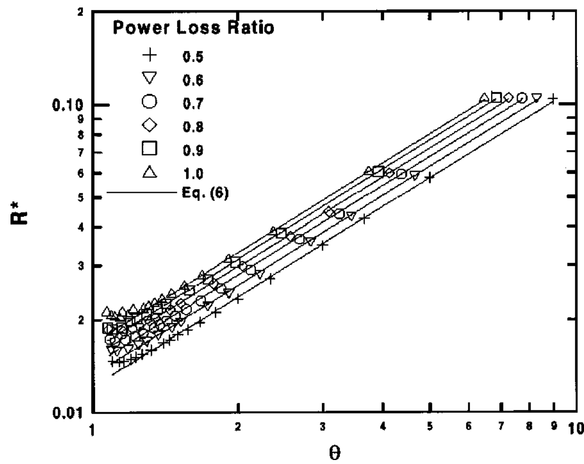

Fig. 5 Comparison between numerical results and general model of ER packages with thermal underfill, Eq. (6)

ER Package with thermal underfill

$$R^* = 1.686\times 10^{-2}\ \ \mathrm{PR}^{0.475}\theta^{0.97}$$
$$0<\theta<\infty \tag{6}$$
$$0.5\leqslant \mathrm{PR}\leqslant 1$$

The standard deviation difference, the average difference and the maximum difference between the numerical results and Eq. (6) are 3.26 percent, 2.75 percent and 15.92 percent, respectively.

ER package without thermal underfill

$$R^* = 1.714\times 10^{-2}\ \ \mathrm{PR}^{0.475}\theta^{0.97}$$
$$0<\theta<\infty \tag{7}$$
$$0.5\leqslant \mathrm{PR}\leqslant 1$$

The standard deviation difference, the average difference and maximum difference between the numerical results and Eq. (7) are 4.04 percent, 4.55 percent, and 17.91 percent, respectively.

Figures 5 and 6 show the comparison between the proposed models Eqs. (6) and (7) and the numerical results. The proposed models for ER surface mount packages with and without thermal underfill can predict the nondimensional thermal resistance within 4 percent. In addition, Eqs. (6) and (7) can predict the surface temperature, T_S, up to 473 K, which is greater than the maximum surface temperature of the thermal class H, where there are no practical applications beyond 453 K. Therefore, the present investigation did not examine any case which has θ lower than 1.10. Moreover, it is evident from Eqs. (6) and (7) that the effect of the thermal underfill material on the nondimensional thermal resistance is around 2 percent. This effect can be considered in the general model as follows

$$R^* = 1.714\times 10^{-2}(k_T/k)^{-0.005}\ \ \mathrm{PR}^{0.475}\theta^{0.97} \tag{8}$$

In general, the available cost effective thermal underfill material is less than 2 W/m.K. Therefore, the maximum reduction of R^* is around 2 percent. Finally, Eq. (8) reveals that $R^*\ \alpha\theta$ ($\theta<1.5$). This means that the thermal resistance is independent of T_∞ in the low range of θ where the dissipated power is transferred by conduction through the package to the substrate. However, for $\theta>1.5$ the dissipated power is transferred by heat conduction through the package to the substrate and partially to the surrounding air. Therefore, one should determine the base temperature in order to estimate T_S. In the coming section the reader will find the empirical equation of T_b based on the experimental results.

Experimental Test and Results

Figure 7 shows the schematic diagram of the experimental setup. The experimental test was conducted inside an environmental chamber to control the air temperature. The ER package was soldered to the FR4 board. The FR4 board and the ER package were covered by a glass reinforced nylon box. This plastic cover simulated the electromagnetic shield and prevented any air circulation inside the environmental chamber to approach the ER package. The surface temperatures of the winding, the core of the ER package and the substrate were measured. The local air temperature, T_∞, inside the plastic box was also measured. The ER14.5 package was used in this test and the dissipated power from this package was calculated from the input DC current and the electric resistance of the winding. The winding resistance was measured at 293 K using Valhalla 4100 ATC and it was 2.503 Ω. The uncertainty in the electrical resistance measurement was around 0.5 percent. However, the local air temperature in the experiment was around 343 K. Therefore, Eq. (9) from Chan [4] was used to correct the resistance at the operating air temperature.

$$R_E = R_{E_{293\ \mathrm{K}}}[1.0+0.0038(T_S-293)] \tag{9}$$

The winding power loss was determined from R_E and the input DC current ($I^2\times R_E$). In this experiment, the uncertainty in the power loss was investigated using the orthogonal error method. It was concluded that the uncertainty in the power loss was ± 10 percent. In addition, there was uncertainty in the measured tem-

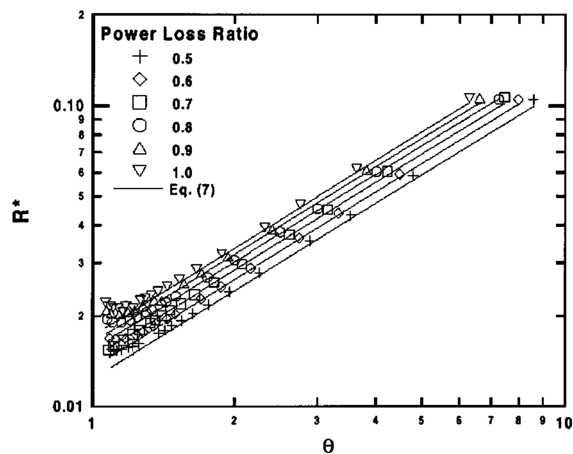

Fig. 6 Comparison between numerical results and general model of ER packages without thermal underfill, Eq. (7)

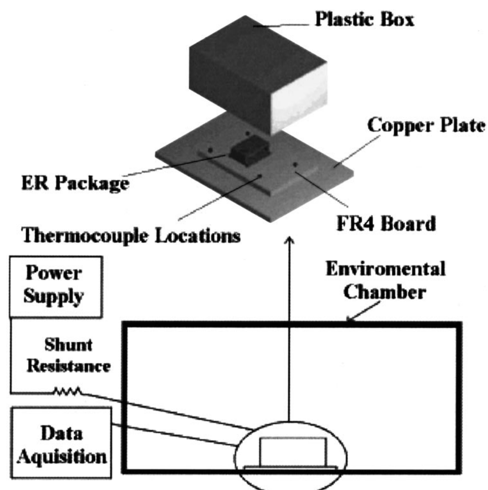

Fig. 7 Schematic diagram of experimental test setup

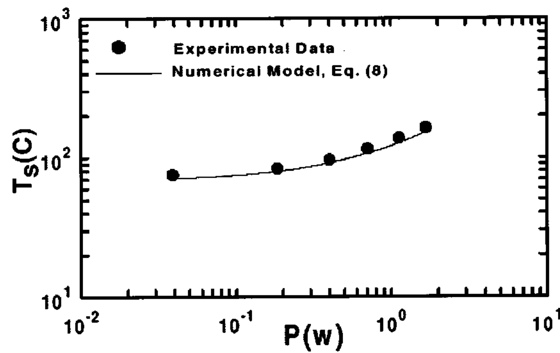

Fig. 8 Comparison between experimental data and general model of ER packages, Eq. (8)

perature by using T-type thermocouple and the attachment of the thermocouple to the component by using the glue in the order of ± 4 percent. Figure 8 shows the relationship between the surface temperature of the ER package windings and the winding power loss. Furthermore, Fig. 8 reveals good agreement between the experimental results and the numerical model, Eq. (8), where $PR=1$ and $k_T/k=1$ (no thermal underfill). The maximum difference between the experimental results and Eq. (8) were 8.4 percent at the highest power loss (2 W) from the ER package. Finally, the present study found that the maximum difference between T_b and T_∞ is a function of the total power, P, as shown in Eq. (10).

$$T_b - T_\infty = 11.42 P^{0.86} \tag{10}$$

Summary and Conclusions

The present investigation conducted a numerical study on gull wing lead ER surface mount magnetic series. This numerical study examined the conduction heat transfer from ER packages to the substrate. The numerical simulation considered the effects of thermal underfill and distributing the power losses between the core and the winding of ER14.5/6 package on the thermal resistance. Moreover, the general conduction heat transfer model for the ER packages were developed based on the numerical results. The model in Eq. (8) has good agreement with the numerical results. The present study concluded that using thermal underfill material to eliminate the air gap between the magnetic package and the substrate is not an effective solution to these types of applications. Moreover, introducing the thermal underfill material in this application can add more unjustifiable costs to the final product. Finally, the present investigation obtained good agreement between the numerical model and the experimental results within a maximum difference of 8.4 percent on the surface temperature.

Acknowledgments

The first author wishes to thank Ms. Miki Narui and Mr. C. Gerolami, Pulse Canada Ltd. and Dr. Elliott Short, Raytheon TI Systems, for their valuable discussions.

Nomenclature

A = total surface area for conduction, m^2
A_C = core surface area for conduction m^2
A_W = winding surface area for conduction, m^2
C_1 = correlation coefficient defined in Eq. (5),
I = DC current, A
K = thermal conductivity of air, W/mK
k_T = thermal conductivity of thermal underfill material, W/mK
m = correlation coefficient defined in Eq. (5),
P = total power losses, $P=P_C+P_W$, W
P_C = core power loss, W
P_W = winding power loss, W
P^* = nondimensional total power losses,
PR = power loss ratio, $PR=P_W/P$
R_E = electric resistance, Ω
R^* = nondimensional thermal resistance,
T = temperature, K
T_b = average substrate surface temperature, K
T_S = maximum surface temperature of ER component, K
T_∞ = ambient air temperature, K
x, y, z = coordinate directions, m
θ = nondimensional surface temperature

References

[1] TDK, 1998, ''TDK's SMD,'' Catalog No. EVE-001, TDK Corporation, Japan.
[2] *Flotherm Instruction Manual*, 1995, Flomerics Limited, Surrey, England.
[3] Dixon, L., 1991, ''Filter Inductor and Flyback Transformer Design for Switching Power Supplies,'' *Unitrode Switching Regulated Power Supply Design Seminar Manual*, pp. M6-1-M6-9.
[4] Chan, Shu-Park, 1993, *Electrical Engineering Hand Book*, Chapter 1, Dorf, R., ed., CRC Press.